Eur. Phys. J. D **37**, 223–229 (2006)
DOI: 10.1140/epjd/e2005-00267-5

THE EUROPEAN PHYSICAL JOURNAL D

An apparatus for studying momentum-resolved electron-impact dissociative and non-dissociative ionisation

V. Sharma and B. Bapat[a]

Physical Research Laboratory, Ahmedabad 380009, India

Received 27 May 2005 / Received in final form 21 July 2005
Published online 4 October 2005 –

Abstract. A spectrometer for recoil ion momentum measurements has been built for studying electron impact ionisation and dissociation of molecules. The apparatus is described in detail, highlighting its capabilities, as well as differences in design from the ones already in use elsewhere. Momentum spectra of ions resulting from 1300 eV electron impact on CO_2 are presented. We observe a broad momentum distribution for the dissociative ionisation reaction leading to the formation of C^+, and two momentum groups in the CO^+ and O^+ channel. By recording multiple ions arising from the same dissociative ionisation event, we also demonstrate the formation of fragment pairs O^+:CO^+, C^+:O^+, and O^+:O^+.

PACS. 34.50.Gb Electronic excitation and ionization of molecules; intermediate molecular states (including lifetimes, state mixing, etc.) – 34.80.Gs Molecular excitation and ionization by electron impact – 39.90.+d Other instrumentation and techniques for atomic and molecular physics

1 Introduction

In the last decade, Recoil Ion Momentum Spectroscopy (RIMS) has come up as a powerful tool in collision studies. Here, besides identification of the recoil-ion species, the recoil momentum vector is completely determined. The idea behind this technique is simple [1,2]. Consider a well-localised and nearly stationary ensemble of target atoms or molecules, ionised by charged particle impact or by absorption of a photon. A uniform electric field guides the ions and electrons formed in the reaction to a position (x, y) on the plane of a detector placed perpendicular to the applied electric field, following a flight of duration t from the instant of the reaction. The motion of the fragments is completely determined by their initial position, the momentum balance in the reaction, and the electric field. Provided the (x, y, t) information is simultaneously registered event-after-event, it is possible to map (x, y, t) onto the three components (p_x, p_y, p_z) of the fragment momentum. This method also enables one to do a kinematically complete measurement of all fragments, giving us unprecedented information on multi-fold differential cross-sections. Momentum spectroscopy offers various advantages over conventional spectroscopy, which can be seen by the wide variety of successfully tackled ion-atom collision, $(\gamma, 2e)$ and $(e, 3e)$ problems. [3–6]. Similar techniques have been successfully implemented for studying fragmentation of molecules. (See [7,8] for comprehensive articles.)

Over the last one-and-half years, we have built a momentum spectrometer for studying molecular reactions. The spectrometer uses the electron-ion coincidence technique for ion time-of-flight measurement and the delay line anode method of encoding the position of arrival of ions on a large diameter channelplate. The spectrometer is now fully functional and a few test experiments have already been undertaken. The design of the apparatus, its capabilities and overall specifications are discussed, following which, momentum spectra of ions resulting from dissociative ionisation of CO_2 are presented.

2 Description of the apparatus

2.1 The ion source

An ion source with a small spatial extent and a low internal temperature is essential for obtaining a good momentum resolution. The primary goal is achieved by having a target-projectile crossed-beams geometry. Usually, a cold supersonic gas beam with very tight collimation is employed, thereby achieving excellent momentum resolution. It is not possible, however, to generate supersonic beams of all gases or liquids. Moreover, if the momenta to be measured are sufficiently larger than the thermal spread of the gas molecules, a supersonic beam is not a must. With these considerations, our set up uses an effusive beam from a capillary of inner diameter 0.15 mm and length 12 mm. A target density of about 10^{13} cm^{-3} is obtained. Besides effusion from the capillary, it is possible to

[a] e-mail: bapat@prl.ernet.in

flood the vacuum chamber through a 6 mm aperture, far away from the ionisation volume, while maintaining the net flow rate. The usefulness of this mode of operation will be made clear later.

Ionisation of the effusive gas is brought about by electron impact, and the electron beam has a focal spot diameter of 0.7 mm at an energy of 1300 eV. The electron gun employs electrostatic focusing and deflection, and an indirectly heated cathode, as found in cathode ray tubes. The gun can be operated in the energy range 600–1900 eV. A 8 cm deep Faraday cup biased at +30 V is used to collect the electrons. In addition to the electron beam, an excimer laser at 308 nm, or an excimer-pumped dye laser (visible wavelengths) can also be used to ionise the target, or polarise and align a molecular target. The ionisation volume for various target-projectile combinations ranges between 1–3 mm^3.

2.2 The ion extraction and drift arrangement

The backbone of the momentum spectrometry technique is the extraction of ions by a uniform, linear electric field over a large volume. A few methods of achieving this appear to have been established. Our design generates a uniform field by co-axially stacking 12 thin aluminium rings, equally spaced, in a potential divider arrangement.

The rings have outer and inner diameters of 200 mm and 100 mm respectively, and are 2 mm thick. Counting away from the central plane, we label the top rings $t_1 \ldots t_6$ and the bottom rings $b_1 \ldots b_6$. The distance between the t_6 and b_6 rings is 220 mm. The b_2 ring (30 mm below the central plane) and the t_6 ring (110 mm above the central plane) have high transmission meshes on them, creating a uniform field over a cylindrical volume of 100 mm diameter and 140 mm height (see Fig. 1). Rings $b_3 \ldots b_6$ are grounded, and are redundant in the present arrangement. Immediately above the t_6 ring is the drift region for ions, defined by a 100 mm diameter tube terminated at the top by a high transmission wire mesh and held at the same potential as the t_6 ring. The drift length of 220 mm, in conformity with the Wiley-McLaren condition ($d = 2s$), nullifies the effect of the spatial spread of the ionisation region on the time of flight resolution [9].

The potential divider arrangement comprises a resistor chain (200 kΩ each) having a low temperature coefficient and tight nominal value tolerance. The measured values of the potentials on the rings are within 0.1% of the notional values. The uniformity of the electric field $\mathcal{E}$, as estimated by computer simulation, is better than 1 in 10^3. The central plane of the stack is at zero potential, and the electron, laser and molecular beams all lie and intersect in this plane. The overlap volume is quite well centred in the extraction volume, as will be seen later. The extraction field accelerates the ions vertically upwards and the electrons downwards. The field strength ranges from 15 V/cm to 80 V/cm. This field is much stronger than that employed in momentum spectrometers for atomic collisions (typically 5 V/cm), thereby leading to a poorer momentum resolution. However, strong fields are essential here, in order that the energetic dissociating fragments can be collected.

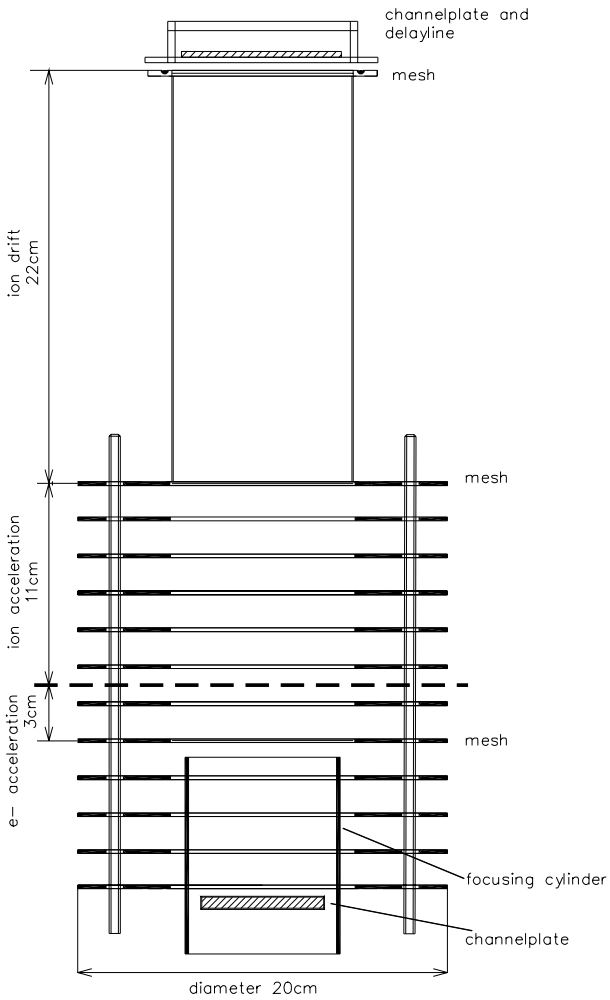

Fig. 1. The momentum spectrometer built for studying molecular fragmentation. The stack of rings for field generation is clearly seen. The compensation ring, discussed in Section 3 is not shown here. The thick horizontal dashed line indicates the plane of the e-beam and molecular beam.

2.3 The ion detector

The ion detector consists of a chevron configuration channelplate with a delay line anode, suitable for rapid position resolved measurement of ions with an estimated resolution of 250 μm and counting rate of about 1 MHz. It has an active diameter of 76 mm. The detector is a commercial design, purchased from Roentdek GmbH. The position encoding is briefly discussed here, details can be found in [10]. The delay line is a bare copper wire wound across opposite edges of an insulating plate. Two crossed pairs of delay lines, isolated from one another, give a 2-D grid. An electron shower (from the back of the channelplate) on this grid causes image-charge pulses to travel to the ends of the wires, giving four pulses for every particle hit. The signals from the channelplate as well as the delay line

anode are fed to non-inverting preamplifiers with a gain between 50–100, and are constant fraction discriminated to generate NIM standard timing pulses. x and y position information is obtained by timing the signals from the two ends of one delay line against each other. The signal from the primary electron shower of the channelplate is used to time the ion arrival. Ion detection and collection efficiency issues are discussed in Section 5.

2.4 The electron detector

The electron detector is a 40 mm diameter channelplate. The use of a channelplate for electrons sometimes leads to ion feedback to the ion channelplate, causing distortion of the image on the ion channelplate. To obtain a satisfactory performance, the electron channelplate has to be moved away from the reaction volume, and a weak barrier potential has to be arranged to suppress the ion feedback. With the increased distance, electron focusing become necessary, which we achieve by introducing a grounded cylinder as shown in Figure 1. The focusing cylinder also reduces stray electron pick-ups. Electron trajectory simulations show that electrons with energies upto 22 eV are collected with 100% efficiency.

2.5 Vacuum and gas handling

The spectrometer is housed in a stainless steel vacuum chamber of diameter 300 mm and height 570 mm, with all-metal joints. Four pairs of cross-ports in one plane permit mounting of the electron gun, the Faraday cup, the laser beam windows and the gas jet. The chamber is pumped by a single 520 lit/s turbomolecular pump backed by a dry scroll pump. The ultimate pressure, achieved after bake-out, is 5×10^{-9} mbar.

Gas is introduced into the chamber either through a capillary, intersecting the path of the electron beam (crossed-beams operation), or through a large aperture far away from the electron beam (flooded operation). The switchover is effected by two all-metal control valves, that are fed through an all-metal fine control needle valve. Once the needle valve is set, the gas leak rate remains constant irrespective of the mode of operation. A pressure gauge monitors the pressure in the stagnation volume between the needle valve and the control valves. In the crossed-beams mode this pressure is about 10^{-1} mbar, and in the flooded mode it is about 5×10^{-3} mbar. The valve and the connecting tubing are kept warm to reduce undesired condensation and clogging.

2.6 Data acquisition

Data acquisition for the momentum spectrometer is based on six timing signals: one from the electron channelplate, one from the ion channelplate and four from the delay line. The ion channelplate signal serves as a master START for every event, triggering five channels of a time-to-digital convertor (LeCroy 133MTD). The first four channels are stopped by the delay line signals, giving the ion position. The fifth channel is stopped by a delayed electron channelplate signal, giving the ion TOF. The TDC has a 500 ps resolution, and a 32 μs range. Digitised outputs of the five channels are read event after event, and stored as a list on a computer disk. The event rate for the present measurement is around 250 Hz, but it is possible to go upto about 1.2 kHz with all channels active.

3 Optimisation of the spectrometer

There are three aspects to optimisation of the spectrometer: tuning the electron beam for proper overlap with the gas beam, locating the overlap correctly w.r.t. the spectrometer axis to obtain proper position and TOF spectra, and filtering out events that may lead to erroneous momentum analysis.

3.1 Electron beam — gas beam overlap

The electron beam can be swept in the transverse direction by electrostatic deflectors. At the focal spot the sweep is about ± 20 mm. The focal length can also be varied between 150–200 mm from the exit aperture. At the energy over which the gun is operated, the earth's magnetic field does not seriously affect its behaviour. Nevertheless, the gun itself is enclosed in a mu-metal cylinder and is aligned approximately along the horizontal component of $\mathbf{B}_{\mathrm{earth}}$. Care is taken to eliminate magnetic materials in the vicinity of the spectrometer. Coarse tuning of the beam is done by observing the beam spot on a fluorescent screen, and fine tuning is done on the basis of the time-of-flight and position spectra. An atomic gas (e.g. argon) is used for this purpose, so that there is a negligible momentum width of the ions. It is important to ensure that the overlap of the electron beam and the molecular beam occurs within about 0.5 mm of the axis of the spectrometer in order to obtain high coincidence efficiency. The position of the overlap along the extraction axis is equally critical, in order to meet the time-focus condition, $d = 2s$.

Since the electron beam enters the spectrometer normal to the extraction field, it suffers a deviation. A 1300 eV beam suffers a deviation of 4–20 mm at the target, for extraction fields between 15–80 V/cm. Even with the extraction field on, it is possible to position the beam on the target, by changing its entry angle. However, this leads to a large number of secondary electrons due to the beam grazing the extraction ring. Furthermore, the beam is not properly collected by the Faraday cup. To get around this problem, we have introduced a ring electrode, which partially compensates for the effect of the extraction field on the e-beam. This ring has inner diameter 80 mm and outer diameter 190 mm, and is placed between the central plane and the b_1 ring. It provides an upward acceleration to the e-beam twice during its transit through the spectrometer. By tuning the compensating electric field and the beam entry angle, it becomes possible to transport the beam

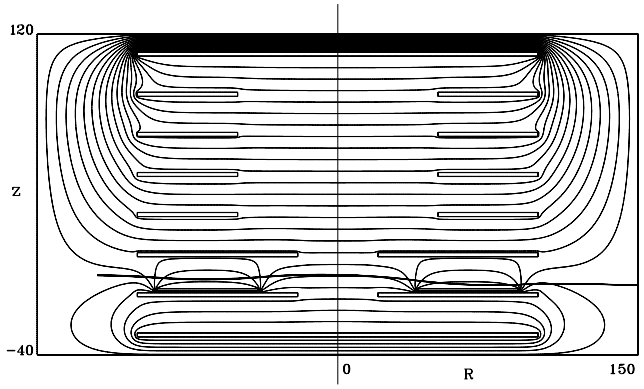

Fig. 2. Trajectory of a 1300 eV electron beam through the extraction stack with the compensation ring. The extraction field is 50 V/cm, and the compensation ring produces an opposing field of approximately the same magnitude. Distances are in mm.

without loss to the Faraday cup, while simultaneously intersecting the gas beam, as seen from a computer simulation (Fig. 2). To minimise the distortion of the extraction field due to the compensation field, the inner diameter of the t_1 and b_1 stack rings is reduced to 40 mm. The uniformity of the extraction field around the ionisation volume remains unaltered to within 1%, while the effective open area for transport of ions remains unchanged.

3.2 Filtering of the raw position and TOF spectra

The TOF spectrum carries the m/q and p_z information, while the position spectrum carries the p_x and p_y information. Only those events for which both x, y and TOF values are recorded can be used for complete momentum analysis. This condition typically eliminates about 80% of the data. A robust momentum analysis is made possible by the application of two more criteria: the position encoding should be well-defined, and the ionisation event should have arisen from a small, well-defined reaction volume.

The first criterion is met by the following consideration. The difference between the time of arrival of the pulses at the ends of the delay line is related to the position of the ion hit, while the sum of the arrival times of the pulses w.r.t. the primary electron shower is a constant for the delay line. The sum distribution shows a peak with a base width of 7 ns for a propagation time of 98 ns, besides some scatter. The distribution is used as a check for genuine events; only those events which fall under the peak are used. This leads to a further 8–12% loss of events, but a high-contrast ion detector image (peak-to-background ratio of over 100) is obtained for the fully determined event list.

The second criterion is met by the following subtraction procedure. Two acquisitions, one in the flooded mode and one in the crossed-beams mode, are made for a specific target and electron energy combination. In the crossed-beams mode, most but not all, ionisation events take place in a small volume located approximately on the spectrometer axis. In the flooded mode, ionisation takes place all along the electron beam trajectory. The difference between the spectra in the crossed-beams and flooded modes can be taken to arise from a well-defined volume. It has been shown that this technique improves the mass resolution of a TOF mass spectrum substantially, if the capillary has a suitable diameter and aspect ratio [11]. To the best of our knowledge, this is the first application of the technique to momentum spectra.

Some caveats are in place while employing the subtraction technique for momentum spectra. Subtraction is only meaningful for distributions, not event lists, so the momentum distribution of each ion species, in the crossed-beams as well as the flooded mode, needs to be separately generated.

The first step is the identification of the ion species, and its $p_z = 0$ point in the TOF spectrum. To this end, the TOF spectrum of an atomic gas like argon is recorded in the crossed-beams mode. The mean positions of the Ar^+, Ar^{2+} and Ar^{3+} TOF peaks are taken to be $p_z = 0$ points. A linear fit of these TOF points to $(m/q)^{1/2}$ provides the m/q calibration and $p_z = 0$ position for *all* ion species.

The second step is the setting of a window on the crossed-beams TOF spectrum for the ion of interest. The same TOF window condition is applied to flooded mode events. We thus obtain a completely determined event list corresponding to the chosen m/q, for both modes. The ion momentum components for each event in the filtered list of the two modes are separately calculated and histogrammed. Finally, the flooded mode momentum histogram is subtracted from the crossed-beams momentum histogram after normalisation for the integrated gas flux and electron current. The subtracted momentum spectrum is taken to be the true spectrum.

4 Results on CO_2

All results discussed here are for 1300 eV electron energy and 60 V/cm extraction field. The gas used here is obtained by purifying commercial grade CO_2 through freezing and distillation. The first distillation stage is at 253 K, at which stage water remains as a frozen residue. The distillate now contains CO_2, N_2 and O_2. A second distillation is done at 77 K, in which N_2 and O_2 are pumped out and pure CO_2 in solid form is obtained. Serious errors can occur in measurements concerning O^+ (due to the contribution from DI of H_2O) and CO^+ (due to its indistinguishability from N_2^+) if this care is not taken.

4.1 Momentum spectra of dissociative ionisation fragments

We first discuss the momentum resolution of our instrument. Throughout this section, atomic units are used for momenta (one a.u. of momentum is the RMS momentum of an electron in the ground state of the H-atom, in units of $|e| = m_e = \hbar = 1, c = 1/\alpha$, and equals 2.04×10^{-24} kg m/s). The instrumental resolution for the

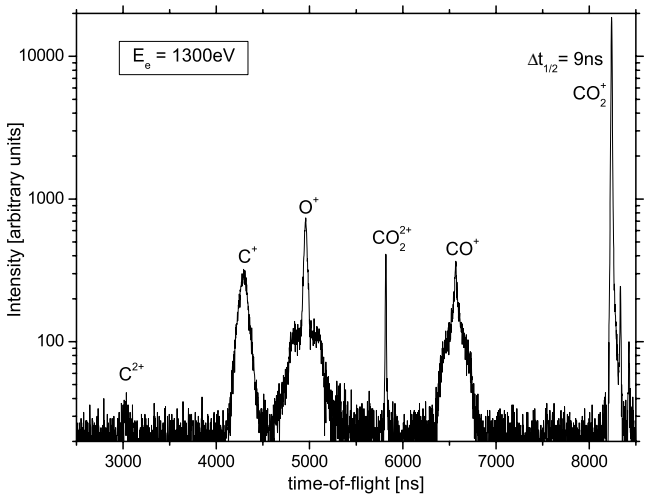

Fig. 3. TOF mass spectrum of ions arising from 1300 eV electron-impact on CO_2, after subtraction of the flooded mode contribution, as explained in Section 3.2.

x (or y) component of the momentum is given by

$$\Delta p_x = m\Delta x/t$$

where Δx is the position resolution of the detector, which is 0.25 mm in the present case, and t is the time-of-flight. We find $\Delta p_x = 2.1$ a.u. for CO_2^+.

The instrumental limit for the momentum resolution of the z component is governed by the time-of-flight resolution and is approximately given by

$$\Delta p_z = q\mathcal{E}\Delta t$$

where $\mathcal{E}$ is the extraction field and q is the ion charge. This works out to be 2.4 a.u.

The achievable resolution is obtained by combining the instrumental width with the thermal width for CO_2 molecules, which is 12.4 a.u. at room temperature. It is thus clear, that in the present set-up, the achievable resolution is limited purely by the thermal width. It should however be noted, that the resolution of the z-component alone is higher, since the effusion of the gas molecules is perpendicular to the z-axis. For CO_2^+, the p_z half-width is found to be 4.3 a.u. while for the total momentum p the half-width is 14 a.u.

Figure 3 shows a time-of-flight spectrum of ions arising from ionisation of CO_2. The width of the CO_2^+ peak may essentially be taken to be the limit of mass resolution. The FWHM of the CO_2^+ TOF peak is 9 ns, while the modal time-of-flight is 8245 ns. This gives a mass resolution $M/\Delta M = 458$. For a given ion peak, the shape of the peak may be approximately taken to be the distribution of the p_z component.

Figure 4 shows the x-y position spectra of three major fragment ions: C^+, O^+ and CO^+. Except for a change of scale, these spectra are essentially the corresponding p_x-p_y spectra. We see clearly that the overall features of the three momentum components are similar for the fragment ions, suggesting a more or less isotropic fragmentation.

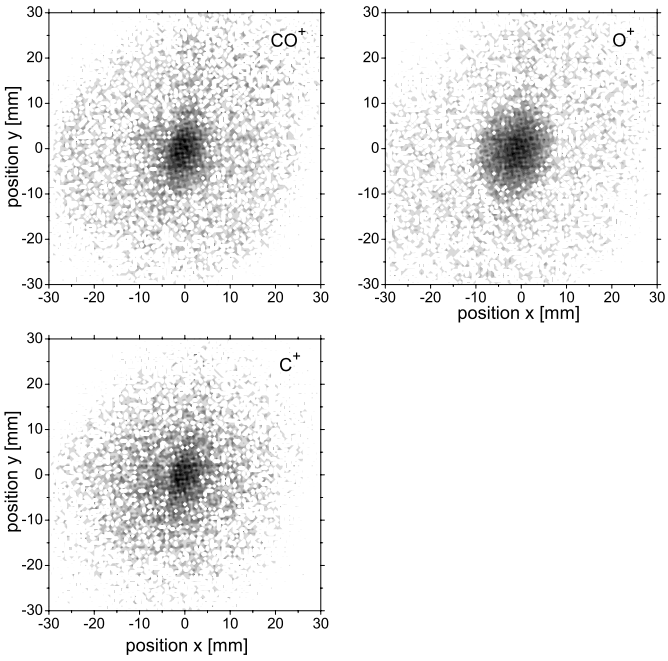

Fig. 4. Position spectra of the three main fragment ions arising from 1300 eV electron-impact on CO_2, obtained by filtering of raw data and subtraction of flooded mode contribution, as explained in Section 3.2.

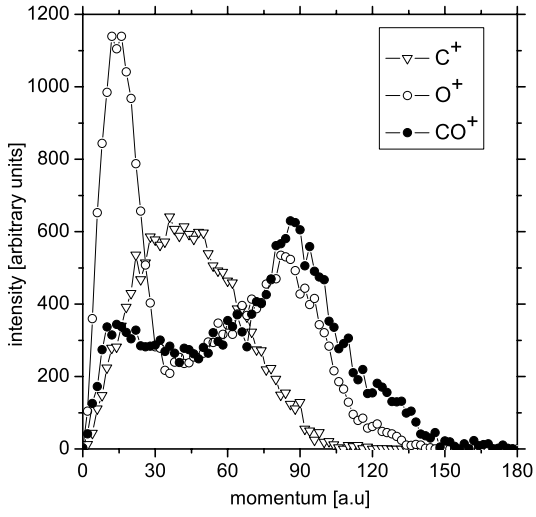

Fig. 5. Momentum distribution of C^+, O^+ and CO^+ ions arising from 1300 eV electron-impact on CO_2.

Momentum spectra (scalar values) for C^+, O^+ and CO^+ ions at 1300 eV electron impact are shown in Figure 5. As would be expected, the C^+, O^+ and CO^+ ions formed by dissociative ionisation carry large momenta as compared to CO_2^+. Two distinct groups are seen in the momentum distributions of CO^+ and O^+. The two momentum peaks occur around 10 a.u. and 90 a.u. for CO^+, and around 14 a.u. and 90 a.u. for O^+.

For O^+, the peak at low momentum is stronger, indicating that there are channels other than two-body breakup leading to O^+. Occurrence of the second peak at the

same momenta for both CO^+ and O^+ indicates, that the same molecular-ion state leads to those O^+ and CO^+ ions which comprise the second peak.

The kinetic energy release (KER) corresponding to the two modal momenta are 0.1 eV and 5.9 eV. This is based on the assumption that most of the CO^+ and O^+ arise from two-body break up. This KER is comparable to typical electronic energy level separations in small molecular ions like CO_2^+. Thus, these structures could be due to dissociation from different electronically excited states of $CO_2^{+\star}$. There may also be a partial contribution from dissociation of $CO_2^{++\star}$. The latter contribution can be separated by the ion-ion coincidence method described in the next section.

The C^+ ion shows a single broad peak. It is likely that C^+ is formed either from a bent-mode vibrationally excited state of CO_2^+ or sequential break-up of a multiply-charged CO_2 ion. The tiny C^{2+} peak has not been momentum analysed due to poor statistics.

4.2 Ion-ion coincidence

Several dissociative ionisation channels are open in the present collision system. We note here a few, which have $CO_2^{++\star}$ as an intermediate state.

$$CO_2 + e^- \rightarrow CO_2^{++\star} + 3e^- \quad (1)$$
$$CO_2^{++\star} \rightarrow CO^+ + O^+ \quad (2)$$
$$\rightarrow C^+ + O^+ + O \quad (3)$$
$$\rightarrow C + O^+ + O^+. \quad (4)$$

At $E = 1300$ eV, the energy transfer to the target is small, and the cross-section for the above reactions is low [12], even lower than that for double ionisation of CO_2. We have been able to observe these reactions, and the fragment ions are recorded in an ion-ion coincidence. The same spectrometer configuration is employed, but the TDC is operated in a multi-hit mode, triggered by a common electron start. Only TOF information is stored. The spectrum of two ion stops is plotted as a t_A vs. t_B contour plot (Fig. 6). The scatter along the forward diagonal is an effect of occasional double-pulsing in the electronics. We see a clear set of contours corresponding to flight times of CO^+ and O^+, indicative of the two-body break-up (Reaction (2)). The elongation of the contour along the $t_A + t_B = 0$ diagonal indicates breakup into two large momentum fragments. The maximum kinetic energy obtained from the extent of this contour is 8 eV for O^+ and 4.5 eV for CO^+. The C^+:O^+ pair is also observed at lower intensity. The shape of this island is consistent with the fact that this ion pair can arise only from a three-body break-up. In addition, we also observe a coincidence between two O^+ ions. They form an asymmetric island in the t_A vs. t_B plot, and one concludes that they are emitted with large momenta (only p_z is recorded here) in the forward-backward directions. The kinetic energy obtained from the forward-backward TOF difference is 9.0 eV. At lower collision energies, Tian and Vidal [12] have observed several ion pairs.

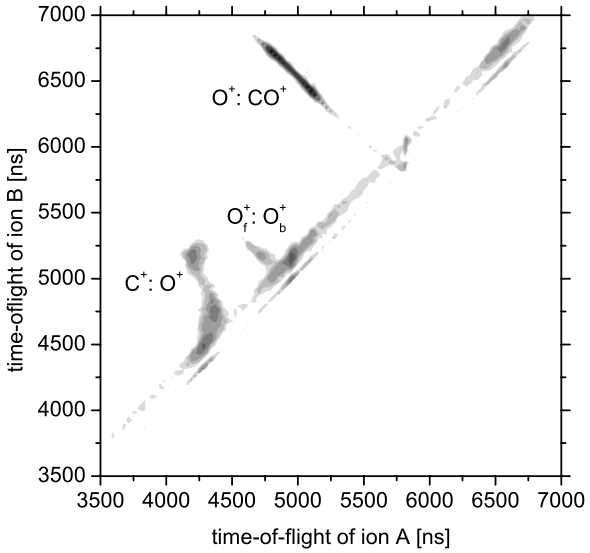

Fig. 6. Coincidence map of flight time of ion pairs arising from 1300 eV electron-impact on CO_2.

5 Further considerations concerning cross-section measurements

Several factors that may lead to misinterpretation of cross-section data (momentum-resolved, or otherwise) need to be looked into, even if absolute values are not desired. Absolute partial cross-sections for electron impact ionisation of CO_2, upto 1000 eV impact energy, can be found in [12,13].

The three major issues are (a) loss of high kinetic energy fragments during transmission (b) bias against low impact velocity ions in conversion to a signal pulse by the channelplate detector (c) loss of genuine TOF coincidences due to poor electron collection.

The first of these factors applies especially to light dissociation fragments. The lightest ion in the present experiment is C^+. Since the electric fields in the spectrometer are linear and uniform, a computer simulation of the trajectories of energetic ions gives an excellent estimate of the cut-off energy. Simulations suggest that with 60 V/cm extraction, all C^+ ions upto 7 eV kinetic energy, irrespective of the direction of emission, are transmitted. The validity of this estimate is borne out by the fact that the highest kinetic energy determined from the momentum spectra of C^+ ions is 7.2 eV. Likewise, complete transmission is achieved for O^+ ions upto 8.5 eV and CO^+ ions upto 11 eV.

The second factor is addressed by choosing argon as the target gas and measuring the ratio of the ion yields Ar^{2+}/Ar^+. This ratio is a sensitive measure of the efficiency of conversion of particle impact into a signal pulse by the channelplate. By varying the channelplate front voltage, the impact energy of the ions is varied, leading to a change in the efficiency of detection. Beyond a certain voltage, the ratio is expected to become a constant. We are limited in the present set-up to to a front bias of about –3900 V. All measurements are performed at this voltage.

For 1000 eV electron impact, our Ar^{2+}/Ar^{+} ratio is found to be 0.073, to be compared with 0.047 of Rejoub et al. [14] and 0.058 of Krishnakumar and Srivastava [15]. This indicates a discrimination in our spectrometer against large m/q ions.

The third factor is rather difficult to estimate. In a manner similar to the ion trajectories, electron trajectory simulations were performed, which show that electrons with kinetic energies upto 22 eV are completely detected, irrespective of their emission direction. Electrons with energies upto 27 eV, emitted in the hemisphere towards the electron detector, are transmitted completely. Since about 70% of the cross-section at high impact energies is dominated by soft electrons, we may roughly estimate that fast electrons emitted away from the electron detector, comprising about 15% of the total electron yield are not detected in our spectrometer.

6 Summary and future plans

In summary, a momentum spectrometer has been built and tested. Momentum-resolved measurements of all fragment ions resulting from dissociative ionisation of CO_2 have been made. Two distinct momentum distributions are seen for the two dominant DI channels leading to CO^{+} and O^{+}. Coincident detection of two ions arising from the same event has also been successfully performed. The CO^{+}:O^{+} fragmentation channel has been identified and an estimate of the kinetic energy release has been obtained. A broad kinetic energy distribution is observed for C^{+}. The ion is also observed in coincidence with O^{+}, indicating a three-body break-up. However, this channel is found to contribute only weakly to the total C^{+} yield.

In the near future, measurements on larger molecules with a view to understanding dissociation pathways are planned. We also intend to use an excimer–dye laser to orient the molecules and obtain momentum-resolved cross-sections for all dissociation channels. Momentum-resolved ion-ion coincidences will enable us to map the levels of excited states of molecular ions. To improve the momentum resolution of the apparatus we plan to replace the gas capillary with a microcapillary array. The possibility of reduction of the spatial extent of the ionisation volume will also be explored. We are also considering the deployment of a supersonic target beam.

Ion-ion coincidences will be looked into in greater detail. Work has already started on obtaining complete momenta for multiple ion hits (upto 4), as opposed to just one component reported here. This will help us in precisely identifying intermediate molecular ion states.

The authors sincerely thank their colleagues in the group, K.P. Subramanian, R.K. Singh, I.A. Prajapati, A.P. Gohil and V.K. Lodha, for their continuous assistance in the setting up of this apparatus and for their constructive criticism and encouragement. They also acknowledge with thanks the generous support of the staff of the mechanical workshop of the laboratory. Timely help from O. Jagutzki and K. Ullmann-Pfleger of Roentdek GmbH is also acknowledged.

References

1. R. Moshammer, M. Unverzagt, W. Schmitt, J. Ullrich, H. Schmidt-Böcking, Nucl. Instr. Meth. B **108**, 425 (1996)
2. J. Ullrich, R. Moshammer, R. Dörner, O. Jagutzki, V. Mergel, H. Schmidt-Böcking, L. Spielberger, J. Phys. B **30**, 2917 (1997)
3. R. Moshammer, J. Ullrich, H. Kollmus, W. Schmitt, M. Unverzagt, H. Schmidt-Böcking, C.J. Wood, R.E. Olson, Phys. Rev. A **56**, 1351 (1997)
4. R. Dörner, H. Bräuning, J.M. Feagin, V. Mergel, O. Jagutzki, L. Spielberger, T. Vogt, H. Khemliche, M.H. Prior, J. Ullrich, C.L. Cocke, H. Schmidt-Böcking, Phys. Rev. A **57**, 1074 (1998)
5. A. Dorn, R. Moshammer, C.D. Schröter, T.J.M. Zouros, W. Schmitt, H. Kollmus, R. Mann, J. Ullrich, Phys. Rev. Lett. **82**, 2496 (1999)
6. B. Bapat, R. Moshammer, S. Keller, W. Schmitt, A. Cassimi, L. Adoui, H. Kollmus, R. Dörner, Th. Weber, K. Khayyat, R. Mann, J.P. Grandin, J. Ullrich, J. Phys. B **32**, 1859 (1999)
7. K. Ueda, J.H.D. Eland, J. Phys. B **38**, S839 (2005)
8. *Imaging in Molecular Dynamics*, editey by B. Whitaker (Cambridge University Press, 2003)
9. I.H. Wiley, W.C. McLaren, Rev. Sci. Instr. **26**, 1150 (1955)
10. O. Jagutzki, V. Mergel, K. Ullmann-Pfleger, L. Spielberger, U. Meyer, R. Dörner, H. Schmidt-Böcking, *Imaging Spectroscopy IV, Proceedings of International Symposium on Optical Science Engineering and Instrumentation*, edited by M.R. Descour, S.S. Shen, Proc. SPIE **3438**, 322 (1998); see also `http://www.roentdek.com`
11. B. Bapat, E. Krishnakumar, Rap. Commun. Mass Spectrom. **9**, 199 (1995)
12. C. Tian, C.R. Vidal, Phys. Rev. A **58**, 3783 (1998)
13. H.C. Straub, B.G. Lindsay, K.A. Smith, R.F. Stebbings, J. Chem. Phys. **105**, 4015 (1996)
14. R. Rejoub, B.G. Lindsay, R.F. Stebbings, Phys. Rev. A **65**, 042713 (2002)
15. E. Krishnakumar, S.K. Srivastava, J. Phys. B **21**, 1055 (1988)